EPJ Web of Conferences 346, 03008 (2026) https://doi.org/10.1051/epjconf/202634603008
RFPPC2025

Application of Solid-state High-power Microwave Source in MPCVD Reactor

Liang Zhu[1*], *Wendong* Ma[1*], *Qiyun* Zhou[2], *Zege* Wu[1], *Lianmin* Zhao[1], *Mao* Wang[1], *Jiafang* Shan[1], *Fukun* Liu[1], *Zhu* Zhou[2], and EAST LHCD Working Group[1]

[1]Institute of Plasma Physics, Chinese Academy of Sciences, Anhui Hefei 230021, China
[2]Hefei Fandao Electronic Technology Co., Ltd., Anhui Hefei 230061, China

Abstract. Microwave Plasma Chemical Vapor Deposition (MPCVD) is the preferred method for producing high-grade diamond due to its electrode-free discharge and pure plasma advantages. With semiconductor advancements, demand for large-size optical-grade diamond is surging. 915 MHz MPCVD, offering 2-3 times larger deposition area than 2.45 GHz systems, is key for large-scale production. However, existing 915 MHz equipment relies on magnetrons, which suffer from high voltage, limited lifetime, and inflexible control. Solid-state microwave sources (low voltage, long lifespan, flexible control) are therefore attractive alternatives. While solid-state amplifiers with output powers of tens of kilowatts are already available in industry, reports at 915 MHz remain scarce, particularly in the context of MPCVD. In this work, we addressed challenges of multi-amplifier branch consistency and high-power radial combining, achieving stable 915 MHz/20 kW output. Preliminary plasma discharge has also been demonstrated, supporting the feasibility of developing large-scale diamond production equipment.

1 Introduction

Artificial diamond synthesis primarily employs High Pressure High Temperature (HPHT) and Chemical Vapor Deposition (CVD) methods. HPHT is limited to small-particle single-crystal synthesis (<3 mm) with inherent defects including low purity (>100 ppm impurities), restricted morphology, and doping challenges [1], failing to meet industrial requirements. In contrast, CVD enables both single-crystal and polycrystalline diamond growth [2]. Key CVD techniques include Plasma-Enhanced CVD (PECVD) and Microwave Plasma CVD (MPCVD). PECVD utilizes vertical electric fields to promote directional growth of carbon nanomaterials while lowering reaction temperatures [3].

MPCVD generates high-energy plasma glow from pure H_2 under microwave excitation, dissociating precursor gases (CH_4, C_2H_2) into free C/H atoms that deposit on substrates [4]. MPCVD technology leverages electrode-free microwave discharge to produce contamination-free plasma, avoiding electrode pollution inherent in Hot Filament CVD (HFCVD) and Direct Current Jet CVD (DCCVD). This makes MPCVD the preferred method for optical-grade diamond synthesis.

However, MPCVD faces a critical limitation: extremely low deposition rates (<3 μm/h for high-quality large-area films [5]), resulting in prohibitive costs that hinder industrial adoption [6]. Research confirms that deposition rate and quality depend fundamentally on active hydrogen atom concentration in plasma, which scales with microwave power density [6]. Conventional approaches boost power density by increasing deposition pressure to compress plasma volume, but this: Reduces plasma diameter by 30-50% [7] Caps diamond growth area at < Ø100 mm. To balance rate and size, simultaneous increases in microwave power (>20 kW) and deposition pressure are essential, necessitating high-power MPCVD systems [6]. Optical-grade large-diameter diamond production particularly requires high-power microwave plasma generators—a technology gap in China, where core equipment relies on imports [6-11].

Driven by semiconductor advancements, optical-grade diamond—nature's highest thermal conductivity material—has emerged as the fourth-generation semiconductor substrate after SiC and GaN. With >6-inch SiC/GaN wafers now mass-produced, cost pressures intensify demand for large-diameter diamond. Conventional 2.45 GHz MPCVD systems max out at ~3-inch diamonds, while 915 MHz systems offer 2-3 times larger deposition areas, making 915 MHz MPCVD development urgent.

Existing 915 MHz MPCVD equipment worldwide relies on magnetrons. Despite their technical maturity, magnetrons require high-voltage operation, which mainly adds to system complexity. More importantly, they are limited by finite lifetimes (due to filament degradation) and inflexible control, which increasingly constrain large-diamond development. In contrast, solid-state microwave sources—featuring low-voltage operation, >50,000-hour lifespans, and agile control—are progressively replacing magnetrons in accelerators and colliders, and represent a promising alternative for MPCVD systems.

Such high-power systems require the coherent combining of dozens of solid-state amplifier branches, where phase–amplitude consistency critically determines combining efficiency and is often constrained by traditional combiners. In this work, our team has overcome multi-branch consistency challenges, enhanced the power capacity of high-frequency radial

* Corresponding author: mwd@ipp.ac.cn

combiners, and achieved a stable 20 kW power output at 915 MHz. When coupled with a custom cylindrical reaction chamber, the system successfully demonstrated plasma ignition, providing a pathway toward next-generation diamond synthesis.

2 Characteristics of the Solid-State Microwave Source System

Operating at 900-930 MHz with a 24 kW power capacity (rated output:20 kW), this solid-state microwave source system integrates an excitation source, two-stage power dividers, 24 driver modules, and 24 × 1 kW power amplifiers, culminating in a 24-way radial combiner for coherent power synthesis. The architecture further incorporates precision control systems, industrial-grade power supplies, and high-efficiency liquid cooling subsystems, with the complete configuration depicted in Fig. 1.

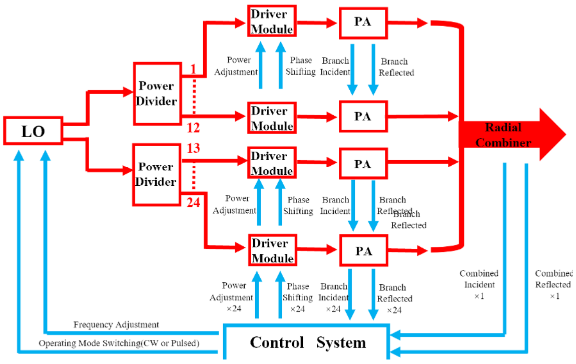

Fig. 1. Block diagram of 915 MHz/20 kW.

The key technical specifications of this solid-state microwave source system are summarized in Table 1, and its primary functional modules will be described in detailed in subsequent sections.

Table 1. Table 1: Key Specifications of the 20 kW Solid-State Microwave Source

Frequency	900 - 930 MHz
Power output	0 - 20 kW
Pulse length	cw
Phase adjustment	0° - 360°

2.1 The low-power microwave source

The low-power microwave source employs a three-port local oscillator (LO), two 1:12 power dividers, and 24 driver modules (specifications are shown in Table 2). The LO provides three outputs: a phase reference signal port plus two divider-drive ports with independent connections to the dividers. Each driver module integrates a digital phase shifter, a nanosecond-speed switch, and a programmable attenuator. Physical implementations of the LO and driver modules are shown in Fig. 2 and Fig. 3 respectively.

Table 2. Key Specifications of the low-power Microwave Source.

Frequency	900 - 930 MHz
Power output	Max. 28 dBm
Pulse length	cw
Phase adjustment	0° - 360°
Attenuation	-40 dB to -1 dB
Switching speed	≤10 ns

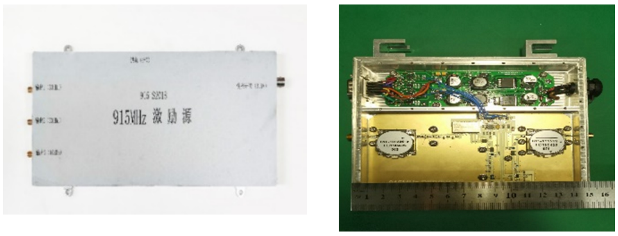

Fig. 2. Left: LO prototype implementation.
Right: microwave driver assembly.

2.2 24×1 kW Solid-State Power Amplifier Modules: Internal Architecture and Liquid-Cooling System

The low-power microwave signal is amplified by 24 × 1 kW solid-state power amplifier modules. As detailed in Fig. 3, each module employs a three-stage amplification scheme: The input signal is first amplified by a 50 W driver stage; The output is split via a two-way Wilkinson power divider to drive dual 600 W power stages; The two signals are combined through a microstrip in-phase combining network to deliver 1 kW output power.

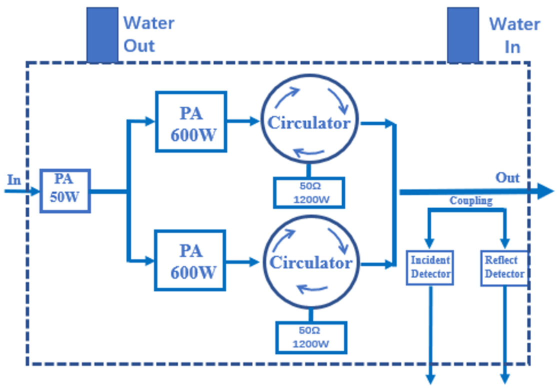

Fig. 3. Circuit architecture of the 1 kW SSPA module.

Considering cost and weight optimization, the water-cooling plate's aluminum alloy main structure incorporates surface-mounted copper thermal bases where the independent 50 W pre-driver and dual 600 W power amplifier modules are installed: amplifier chips are vacuum-reflow-soldered directly to the copper bases while PCBs with immersion gold finishes are bonded to the same bases via pre-placed solder shims under uniform heating; these copper assemblies are rigidly mounted to the water-cooling plate through M4 screw holes with thermal grease (k＞3 W/m·K) applied at copper-aluminum interfaces to balance thermal performance and cost, while friction-stir-welded coolant beneath amplifier chip footprints for targeted heat dissipation enhancement. Fig. 4(a) illustrates the internal coolant channel topology of the cold plate, with Fig. 4(b) showing the corresponding top-view configuration of the cooling module.

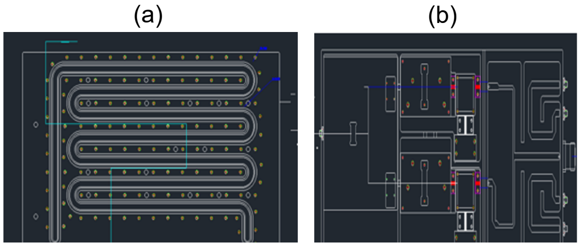

Fig. 4. (a) Internal coolant channel topology of the cold plate. (b) Top-view configuration of the cooling module.

Upon finalization of the liquid cooling topology, thermal simulation must determine the minimum coolant flow rate required to maintain the power amplifier within a safe temperature range. The primary heat sources are two NXP BLF10H6600 power amplifier chips (600 W output each, measured efficiency ≥60%), with total thermal dissipation about 650 W, Although the datasheet permits a maximum junction temperature of 225 °C, reliability derating criteria (per IEC 62368) mandate strict control below 75 °C in engineering practice. Thermal simulations in Fig 5 confirm that a coolant flow rate of 7 tons/hour achieves stable junction temperatures within this 75 °C safety threshold.

The engineering prototype of the 1 kW solid-state power amplifier module is shown in Fig. 6.

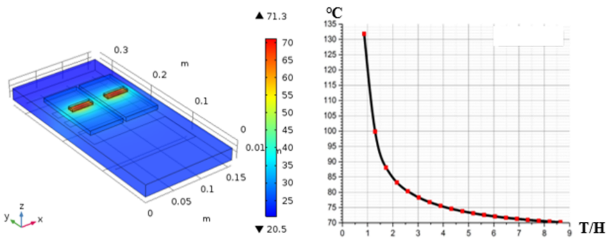

Fig. 5. Left: thermal simulation of water cold plate. Right: temperature vs. water flow.

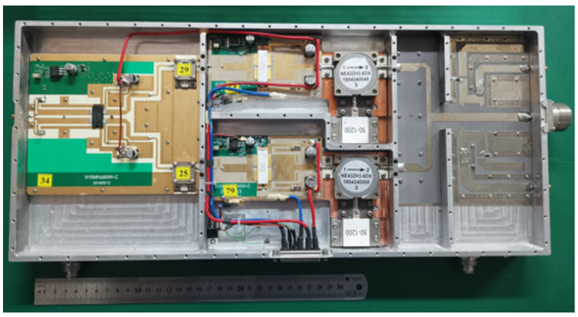

Fig. 6. The engineering prototype of the 1 kW SSPA module.

2.3 High-Power 24-Way Radial Combiner (20 kW)

To address the >15 kW thermal dissipation challenge in conventional combining architectures for twenty-four 1 kW power amplifier modules, we employed the intrinsic single-stage high-efficiency synthesis of radial combiners (theoretical efficiency >98%) via multi-port synchronous injection. Three main technical issues were resolved: (i) the lack of 915 MHz, 20 kW-class radial combiners, (ii) isolation degradation (<20dB) caused by multi-port coupling, and (iii) thermal instability risks near 25 kW. A three-dimensional tapered impedance matching structure improved isolation to 35dB, while a copper–aluminum hybrid microchannel heatsink (thermal resistance 0.03 °C/W) effectively managed thermal dissipation. A 24-way 25 kW radial combiner (900–930 MHz) was thus developed, demonstrating 98.2% combining efficiency and ±0.25dB amplitude consistency. These results provide a technical basis for scaling solid-state microwave sources in MPCVD applications.

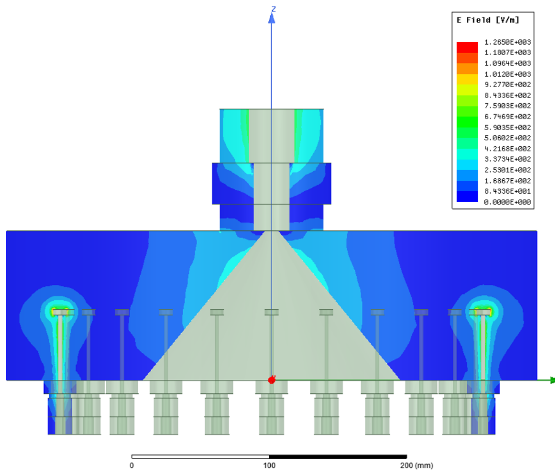

Fig. 7. Overall simulation model of the power combiner.

2.4 Control system

As illustrated in Fig. 8, the hardware architecture of the Solid-State Microwave Control System (MSCS) comprises three core components: solid-state microwave source system, power measurement subsystem, and power control computers. The system acquires power signals via bidirectional couplers, processes data through real-time fitting algorithms in the control computers, and outputs control signals to programmable attenuators within the microwave source system. This enables millisecond-level closed-loop continuous adjustment of power (control cycle: 1 ms), while strictly maintaining power and phase consistency across all amplifier branches.

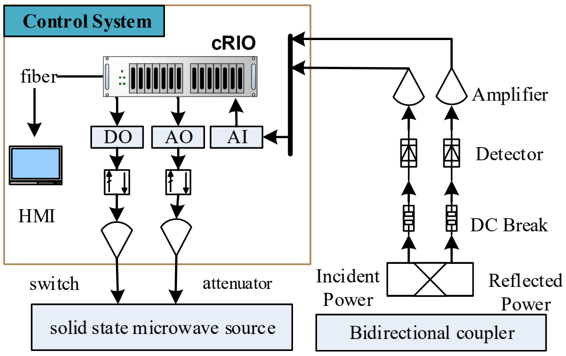

Fig. 8. The hardware architecture of solid state microwave source control system.

The solid-state microwave control system, architected on a National Instruments (NI) platform, integrates a CompactRIO real-time controller (with 8 I/O cards) and a LabVIEW-based industrial HMI touch panel for localized operation. It independently regulates 24 microwave branch powers, with pre-calibration compensating for amplifier inconsistencies to ensure output uniformity. The CompactRIO leverages a user-programmable FPGA and high-speed I/O resources (50 AI, 24 AO, 25 DI channels): AI channels acquire branch/total incident/reflected powers, converting to real-time values via pre-calibrated power-voltage fitting models; AO channels drive attenuators with voltage signals for dynamic power adjustment; DI channels switch microwave outputs via 5V TTL signals.

As depicted in Fig. 9, the software workflow begins with parameter initialization through HMI-shared variables. A start command (start=1) triggers real-time power acquisition (via TCP/IP), concurrently logging data and updating HMI displays. The FPGA compares actual vs. target powers, outputting AO control voltages for closed-loop regulation. Upon stop command (stop=1), the loop halts, with HMI visualizing discharge waveforms for the next cycle.

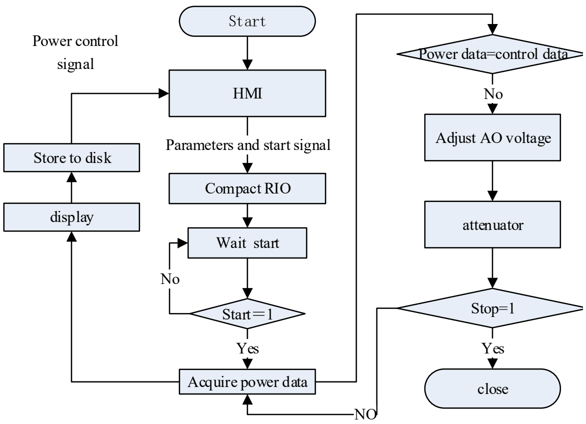

Fig. 9. The software flow chart of control system.

2.5 Power supplies

The ICs operate at 48 V DC, and given the exceptionally high conversion efficiency (>98%) of switching power supplies, the system employs Huawei 48 V/50 A switching power modules. To address the stringent amplitude/phase consistency requirements under 20 kW total power demand while eliminating risks of voltage deviation and power imbalance from independent power sources—and to prevent system instability caused by single-module failures—a centralized redundant power architecture is implemented: Thirty-two power modules are paralleled with an integrated intelligent monitoring system that displays real-time power/current parameters per module and triggers operational alerts, thereby fundamentally eliminating system instability induced by single-point failures. The power system topology is illustrated in Fig. 10.

Fig. 10. The power system topology.

3 Integrated System Implementation and High-Power Characterization

As shown in Fig. 11, the solid-state microwave source system adopts a modular cabinet design (2200×800×1200 mm, H×W×D) implementing a graded thermal zoning strategy for efficient heat dissipation: Top layer: Integrated radial combiner with microchannel liquid-cooling ports; Middle layer: 24 solid-state power amplifier modules with ducted air cooling (maintaining case temperature <65 °C); Bottom layer: Redundant power supply array (20× Huawei 48 V/75 A modules);

Fig. 11. Engineering prototype implementation of 20 kW solid-state microwave source.

This architecture enables stable 20 kW continuous-wave full-power operation (as shown in Fig. 12).

Building upon this foundation, we innovatively developed a high-Q resonant coupling cavity, successfully constructing a complete MPCVD system (Fig. 13) where preliminary plasma discharge was achieved.

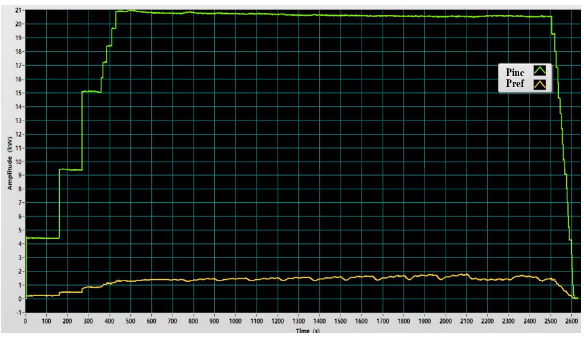

Fig. 12. Performance characterization at 20 kW full-power operation

Fig. 13. 20 kW solid-state MPCVD system @ 915 MHz.

4 Conclusion

After three years of research and development, our team has developed a 20 kW solid-state microwave source system operating at 915 MHz, achieving three significant advances:

(1) 24-channel amplitude–phase consistency control (±0.1dB / ±0.8°);

(2) high-frequency and high-power extension of radial combiners (900–930 MHz / 25 kW capacity, >98.2% efficiency);

(3) thermal management at 20 kW (ΔT < 18.3 °C).

The system provides a highly reliable microwave energy platform for semiconductor manufacturing and demonstrates the technical feasibility of fully replacing magnetrons in 915 MHz MPCVD equipment.

5 Acknowledgments

The authors extend profound gratitude to all colleagues in the LHCD team for their invaluable contributions and dedicated collaboration throughout this research endeavor.

References

1. M. O. Fregeau, S. Oberstedt, T. Brys, et al., First use of single-crystal diamonds as fission-fragment detector, Nuclear Instruments and Methods in Physics Research Section A: Accelerators Spectrometers Detectors and Associated Equipment **791**, 58-64 (2015). https://doi.org/10.1016/j.nima.2015.04.030

2. J. Isberg, J. Hammersberg, et al., High Carrier Mobility in Single-Crystal Plasma-Deposited Diamond, Science **297**, 1670 (2002). https://doi.org/10.1126/science.1074374

3. R. Issaoui, J. Achard, F. Silva, et al. Growth of thick heavily boron-doped diamond single crystals: Effect of microwave power density, Applied Physics Letters, 97, 182101 (2010). https://doi.org/10.1063/1.3511449

4. Q. Liang, C.S. Yan, Y. Meng, et al. Recent advances in high-growth rate single-crystal CVD diamond, Diamond and Related Materials **18**, 698-703 (2009). https://doi.org/10.1016/j.diamond.2008.12.002

5. K. An, X. Liu, X. Li, et al. Numerical Simulation and Experimental Study of a Novel High-power Microwave Plasma CVD Reactor for Diamond Films Deposition, Journal of Synthetic Crystals **44**, 1544-1550 (2015). http://rgjtxb.jtxb.cn/EN/

6. D. G. Goodwin, Scaling laws for diamond chemical-vapor deposition. I. Diamond surface chemistry, Journal of Applied Physics **74** , 6888-6894 (1993). https://doi.org/10.1063/1.355063

7. Q. Liang, Y.F. Meng, C.S. Yan, et al. Developments in synthesis, characterization, and application of large, high-quality CVD single crystal diamond, Journal of Superhard Materials **35**, 195-213 (2013). https://doi.org/10.3103/S1063457613040011

8. J. Weng, L.W. Xiong, J.H. Wang, et al., Investigation of depositing large area uniform diamond films in multi-mode MPCVD chamber, Diamond and Related Materials 30, 15 (2012). https://doi.org/10.1016/j.diamond.2012.09.007

9. L. Wang, Y. Xia, J. Ju, et al., Efficient luminescence from CVD diamond film-coated porous silicon, Journal of Physics Condensed Matter **12**, L257 (2000). https://doi.org/10.1088/0953-8984/12/13/104

10. Q. Fang, L. Wang, Q. Zeng, et al., Preparation and photoelectric properties of a thin-film nanocrystalline diamond phototransistor, International Symposium on Photoelectronic Detection & Imaging: Material & Device Technology for Sensors (2009). https://doi.org/10.1117/12.835508

11. H. Yamada, A. Chayahara, Y. Mokuno, Numerical and experimental studies of high growth-rate over area with 1-inch in diameter under moderate input-power by using MWPCVD, Diamond and Related Materials **17**, 1062 (2008). https://doi.org/10.1016/j.diamond.2008.01.045